Ceramics International 47 (2021) 27342–27350

Contents lists available at ScienceDirect

Ceramics International

journal homepage: www.elsevier.com/locate/ceramint

Dependence of mechanical and tribological performance on the microstructure of (CrAlTiNbV)N_x high-entropy nitride coatings in aviation lubricant

Xiaolong Lu [a,b,c], Cunxiu Zhang [a,d], Xiao Zhang [a,b,c], Xinjian Cao [a,b,c], Jian Kang [a,e], Xudong Sui [a,b,c,*], Junying Hao [a,b,c,**], Weimin Liu [a]

[a] State Key Laboratory of Solid Lubrication, Lanzhou Institute of Chemical Physics, Chinese Academy of Science, Lanzhou, 730000, China
[b] Center of Materials Science and Optoelectronics Engineering, University of Chinese Academy of Sciences, Beijing, 100049, China
[c] Qingdao Center of Resource Chemistry and New Materials, Qingdao, 266000, China
[d] Department of Materials Science and Engineering, China University of Petroleum (East China), Qingdao, 266580, China
[e] School of Mechanical and Automotive Engineering, Qingdao University of Technology, Qingdao, 266033, China

ARTICLE INFO

Keywords:
CrAlTiNbV)N_x coatings
Substrate bias
Wear
Aviation lubricant

ABSTRACT

The (CrAlTiNbV)N_x coatings are fabricated by controlling the substrate bias via magnetron sputtering method. Under low substrate bias, the coating tends to form a loose columnar crystal structure with (200) preferred orientation. However, when the substrate bias increases, the coating transforms into a dense nanocrystalline structure, and the (111) orientation is enhanced. As the substrate bias increases, the residual stress and hardness of the coating gradually increase, while the adhesion strength decreases slightly. Friction tests show that the coating possesses the lowest average friction coefficient (about 0.06) and wear rate (8.7×10^{-9} mm^3/N·m) in 4050# aviation lubricant, which is achieved under the substrate bias of -96 V and -126 V, respectively.

1. Introduction

Nowadays, aircraft engines are becoming an increasingly important role in the aviation industry and are demonstrated to be one of the most sophisticated manufacturing techniques [1]. The inevitable friction and wear problems between the key components of aero-engines, such as spindle bearings, hinges and gears, are urgently needed to be solved at the moment. Fortunately, this challenge gives an impetus for the development of protective coatings which can increase the service life and reliability of moving parts for aviation applications.

Recently, high entropy nitride (HEN) coatings have been widely studied in virtue of excellent mechanical properties, anti-wear properties and good corrosion resistance [2,3]. For example, Xia et al. [4] conducted a study into the effect of N content on the properties of $(MoNbTaVW)_{1-x}N_x$ coatings, and found that the hardness of the coatings reached up around 30 GPa with increasing N content accompanied by a structural change. Lai et al. [5] fabricated (AlCrTaTiZr)N coatings via tuning substrate bias. It was pointed out that the maximum hardness (36.9 GPa) and excellent anti-wear behavior were obtained under a higher bias (-150 V) as a consequence of a change in the microstructure. On the whole, for high-entropy nitride coatings, its mechanical and tribological properties are closely related to its microstructure. In order to optimize the microstructure as well as properties of the coating, two vital parameters, including nitrogen flow rate (gas pressure) [6–8] and substrate bias [9,10], are often adjusted to obtain the desired effect. By changing the nitrogen flow rate during the preparation process, the continuous variation in the coating microstructure can be controlled, which in turn can affect the performance of the coatings. As the nitrogen flow rate increases, the microstructure of the coatings transitions from an amorphous structure to a columnar crystal structure [11]. However, it was discovered that the excessive nitrogen flow rate will weaken the bombardment effect as a consequence of the decreased plasma energy, and thus a porous and loose columnar structure was obtained, which can deteriorate the tribological properties of the coatings [12]. As demonstrated by our research group, the coating with dense and high-cohesive columnar crystals structure can be obtained by adjusting the nitrogen flow rate and thereby improving the tribological properties of the coatings. However, the maximum hardness of the coating does not

* Corresponding author. State Key Laboratory of Solid Lubrication, Lanzhou Institute of Chemical Physics, Chinese Academy of Science, Lanzhou, 730000, China.
** Corresponding author. State Key Laboratory of Solid Lubrication, Lanzhou Institute of Chemical Physics, Chinese Academy of Science, Lanzhou, 730000, China.
E-mail addresses: suixudong@licp.cas.cn (X. Sui), jyhao@licp.cas.cn (J. Hao).

https://doi.org/10.1016/j.ceramint.2021.06.156
Received 24 May 2021; Received in revised form 11 June 2021; Accepted 19 June 2021
Available online 21 June 2021

exceed 18 GPa [13]. Therefore, it is necessary to further densify the coating structure and improve the hardness and wear resistance. Increasing the energy of particles by adjusting the substrate bias is an effective method for coating densification. Wang et al. [14] fabricated the (AlCrSiNbZr)N_x coatings via tuning substrate bias and found that the maximum hardness was achieved at the bias of -75 V. In addition, the (111) orientation was dominated under the substrate bias from 0 V to -75V, while amorphous-like structure was observed at the bias of -100 V. Lo et al. [15] fabricated the (AlCrNbSiTiMo)N coatings by tuning substrate bias and an excellent hardness of 34.5 ± 0.8 GPa was obtained. Besides, the preferred orientation of coatings varied from (111) to (220) as a result of the increasing substrate bias, which can be attributed to the increasing ion channeling effect.

Therefore, in this study, the emphasis is placed on improving the hardness of the coating by tuning bias in the preparation process, and studying the influence of the substrate bias on the microstructure and mechanical properties of coatings. Of equal importance is to explore the tribological properties of the coating owing to the lacking study of solid-liquid composite lubrication in aviation lubricant.

2. Experimental section

2.1. Coatings preparation

The (CrAlTiNbV)N_x coatings are fabricated on silicon (100) wafers (for microstructure characterization), 9Cr18 steel (Ra≤0.05 mm, HRC57) (for measurement of mechanical and tribological properties) and 304 stainless steel (for measuring the residual stress) substrates using magnetron sputtering technique. Before deposition, all substrates are ultrasonically cleaned for 10 min, followed with petroleum ether and alcohol, respectively. After being dried by compressed air, the substrate is fixed on the pre-cleaned sample holder and mounted on the turntable in the vacuum chamber. The working distance from the target to the substrate is about 12 cm, and the rotation speed of the sample holder is set as 5 rpm. When the vacuum chamber pressure reaches 1.0×10^{-3} Pa, the argon is introduced into the vacuum chamber at the moment when the deposition system starts to operate, and the argon flow is set to be 18 sccm. All samples are cleaned using Ar^+ for 30 min for the purpose of removing the surface oxides and contaminants. Then, the Cr bonding layer is preferentially deposited to enhance the bonding force of the coating to the substrate. Finally, a stable nitrogen flow rate (38 sccm) is introduced into the vacuum chamber, and the (CrAlTiNbV)N_x coatings are deposited on the substrate by applying a current of 4.5 A on the CrAlTiNbV target at the substrate bias of -36 V, -66 V, -96 V, -126 V and -156 V, respectively. To facilitate the following discussion, S-36, S-66, S-96, S-126, and S-156 are used to denote the (CrAlTiNbV)N_x coatings prepared under the substrate bias of -36 V, -66 V, -96 V, -126 V and -156 V, respectively.

2.2. Coating characterization

The cross-sectional images of coating microstructures are taken with a scanning electron microscope (JSM-7610F), and the chemical compositions are determined by energy dispersive spectroscopy (EDS, OXFORD). The morphology and surface roughness of the coatings are characterized by AFM equipment (NanoWizard 4). The X-ray diffractometer (D8 ADVANCE) is used to analyze the crystallographic structure of coating and the incident angle is selected as 1°. A substrate-curvature method is taken to determine the residual stress of coatings, which is calculated by Stoney equation:

$$\sigma = -\frac{E_s \cdot t_s^2}{6(1-\upsilon_s)\cdot t_f}\cdot\left(\frac{1}{R_f}-\frac{1}{R_s}\right) \quad (1)$$

where E_s and υ_s belong to the modulus and the Poisson ratio of the 304 stainless steel substrate (50 × 10 × 0.8 mm^3), which is 195 GPa and 0.27, respectively, t_s and t_f represent for the thickness of the steel substrate and film, and R_s and R_f are the radius of curvature of the steel substrate before and after deposition, which can be determined by film stress tester (FST 1000). Nano-hardness measurements (AGILENT, G200) are used to reflect the changes in coating hardness and elastic modulus deposited at different biases. The Berkovich diamond indenter is used in the experiment, where the radius of curvature is 20 nm. To eliminate the effect of the substrate on the hardness of the coating, the measured penetration depth is less than 10% of the coating thickness. In the experiment, the hardness and modulus of each sample are measured by taking the average of 10 measurements, and the Poisson's ratio is selected as 0.23. A scratch tester (MFT-4000) is used to characterize the bonding behavior of the coating. During the test, a loading speed of 100 N/min is used to attain a terminal load of 120 N and a sliding length of 5 mm is taken. To assess the wettability of 4050# oils on the coating surface, the optical images and the contact angle are evaluated using a contact angle measurement instrument (DECCA-100). The tribological behaviors are conducted on a ball-on-disc tribometer (CSM) instruments in air (temperature: 20 °C, relative humidity: 40%) with a total sliding time of 2 h. The 9Cr18 steel ball (Φ6 mm, Ra≤0.05 mm, HRC57) acts as a counterpart. The tests are carried out at the load of 20 N and the line speed is set as 6.28 cm/s. After friction and wear test, the 3D surface profiler (UP-Sigma) is taken to evaluate the wear tracks of the coatings after sliding 2 h. The wear rate (w) is determined by Ref. [16]:

$$w = V/NS \quad (2)$$

where V is the wear volume (mm^3), N is the load (N) and S is the total distance (m).

3. Results and discussion

3.1. Structure and morphology

Fig. 1 depicts the SEM images of (CrAlTiNbV)N_x coatings at varying substrate biases. The Cr binding layer is firstly deposited and the thickness is about 110 nm. With the increase of the substrate bias, the coating becomes denser, and the thickness values of the coatings prepared under different biases are in the range of 0.6–0.83 μm. For the S-36 and S-66 sample, the columnar crystal structure can be clearly observed, and there exist obvious voids between the columnar crystalline caused by the shadow effect during deposition process. That is to say, during the rotation of the sample holder, due to a certain degree of oblique incidence between the substrate surface and the target, atoms will be covered by adjacent atoms. However, the shadowing effect can be eliminated at higher substrate bias thanks to the high-energy particles bombardment, which can suppress the growth of the columnar crystal structure. The microstructure presents a transitional state, which is composed of columnar crystals and fine nanocrystalline structures for the S-96 sample. The coating takes on a highly dense nanocrystalline structure at higher substrate biases (-126 V, -156V). This is because that, the ion bombardment energy increases accompanied by an increase in substrate bias, and the high-energy ions bombard the coating to increase its defects and the number of nucleation sites, which will inhibit the growth of crystal grains and turn the columnar crystal structure into a nanocrystalline structure. In addition, due to the re-sputtering effect, the particles with relatively weak surface binding will be sputtered out, leaving the part that is firmly bonded to the substrate, which can hinder the formation of the columnar crystal structure. According to EDS analysis, the chemical compositions of (CrAlTiNbV)N_x coatings are shown in Table 1.

Fig.2 shows the surface morphology and line roughness (R_a) of (CrAlTiNbV)N_x coatings observed by AFM. As can be seen, all samples possess the dome-shaped surface morphology with different degrees of aggregation and R_a values with respect to substrate bias. As the substrate bias increases, the roughness of the coating surface decreases first, and

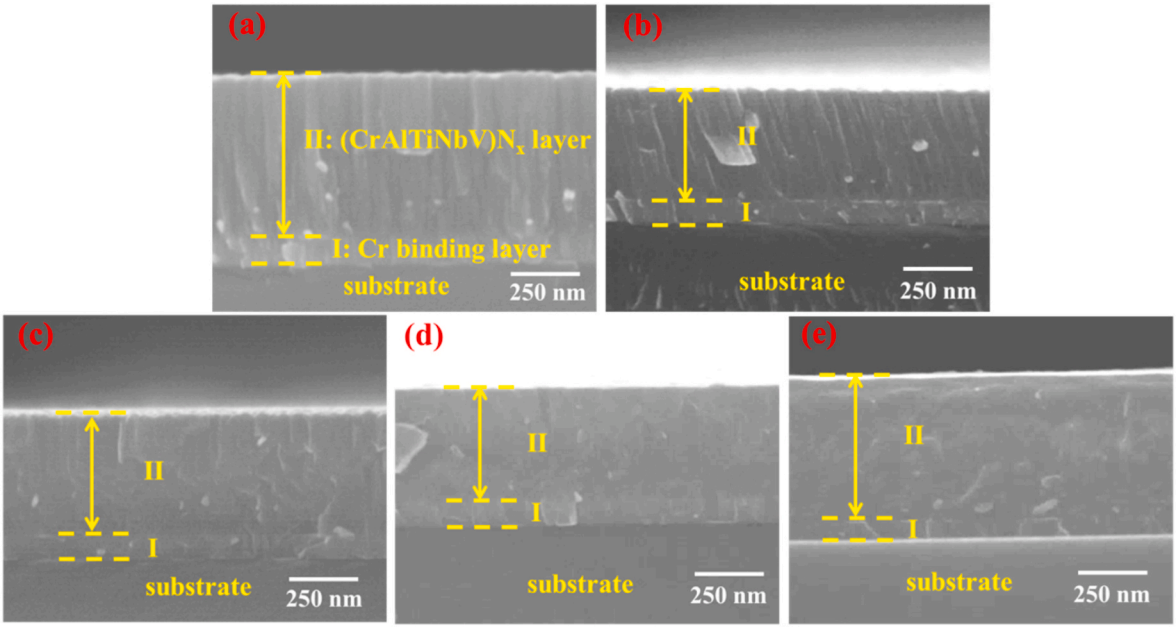

Fig. 1. SEM cross-section images of (CrAlTiNbV)N_x coatings fabricated at various substrate biases: (a) -36 V, (b) -66 V, (c) -96 V, (d) -126 V, and (e) -156 V.

Table 1
The chemical composition of (CrAlTiNbV)N_x coatings.

	Cr	Nb	Ti	Al	V	N
Concentration (at.%)	27.3	7.2	6.5	8.9	9.8	40.3

the S-96 sample reaches the minimum R_a value (2.45 nm), and then increases as the substrate bias continues to increase. The increase in the energy of ions bombarding the coating surface is accompanied by an increase in the substrate bias, and the energetic atoms can smooth the coating surface to a certain extent. However, when the substrate bias continues to increase, high energy bombardment particles can implant the growing coatings, which can generate more defects and thus obtain an uneven coating surface, resulting in a larger surface roughness of the coating. Therefore, the roughness of the coating surface at varying substrate biases is related to the energy of the atoms reaching the surface of the coating. The neutral high-energy argon atoms seem to be collapse the island-like structure and turn it into small particles. However, when the energy reaching the surface atoms is large enough, the aggregation of optimal atomic sites can contribute to a higher roughness [17]. The substrate bias has an impact on the degree of atomic aggregation by which the nucleation and growth mechanism are altered at a higher bias. Moreover, this means that the coating growth is mainly carried out by island formation, which is in accordance with the Volmer-Weber growth mechanism [18].

Fig. 3 illustrates the XRD patterns of (CrAlTiNbV)N_x coatings at varying substrate biases. It is suggested that all samples present simple FCC solid solution structure and all constituent elements are located in the lattice sites of the FCC structure. In previous studies, it can be observed that the high-entropy nitride coating presents a single FCC structure instead of separate nitrides that coexist with each other [19–21]. The difference in the atomic size of each constituent element in the high-entropy nitride will provide high mixing entropy, which is conducive to enhancing the formation of solid solution phase, thereby proving its stability. From the perspective of preferred orientation, all coatings predominantly have a strong (200) orientation, and followed by the (111) orientation. This phenomenon regarding preferred orientation can be linked with thermodynamic and kinetic aspects. From a thermodynamic point of view, it is discovered that the (111) plane possesses the lowest strain energy, the (200) preferred orientation growth owns the lowest surface energy and the (220) owns the lowest stopping energy [22]. The total energy obtained from the sum of strain energy, surface energy, and stopping energy is expected to reach the minimum in thermodynamics [23]. The preferred orientation of nitride coating with NaCl-Type FCC structure is totally determined by the competition between surface energy and strain energy. Hence, the more competitive (200) orientation denoting the lowest surface energy possesses more growth advantages over the (111) with the lowest strain energy for all samples deposited at varying substrate biases. It is easier to achieve the thermodynamic equilibrium deposition state accompanied by the increasing substrate bias, and the increased bombardment energy on the coating surface can be transmitted to the atoms in the coating, thereby increasing the mobility of atoms. Therefore, on one hand, the largest number of atoms per unit area can grow preferentially in the (111) orientation only at low energy sites. On the other hand, surface atoms with higher mobility tend to be oriented at the lowest surface energy plane. Accordingly, the (200) is the preferred orientation under various biases [24]. From the perspective of kinetic aspect, the (111) possesses a more closely packed NaCl structure with the densest array of atom columns, which is most vulnerable to cascading collisions. On the contrary, the (200) and (220) own the most open channel favored by coatings deposited under high-ion-energy conditions [25]. Therefore, due to the anisotropy of the collision effect, the (200) has a higher survival probability than the (111) when facing ion bombardment. It can be seen from Fig. 3 that the peak position of (111) shifts to lower angles with the increase of the substrate bias. This is due to the fact that the energy and flux of ions that bombard the substrate increase as a consequence of the increase in the substrate bias, which results in the increase in the lattice parameter of the coating [26].

3.2. Residual stress

Fig. 4 exhibits the residual stress of (CrAlTiNbV)N_x coating versus substrate bias. As can be seen, the (CrAlTiNbV)N_x coatings prepared via magnetron sputtering exhibit a large compressive residual stress originated from energetic ion bombardment. The compressive residual stress of the coating gradually increases (-0.3 to -7.5 GPa) accompanying the increase of the substrate bias, and the S-126 sample owns the largest residual stress, while the residual stress of the coating decreases slightly as the bias continues to increase. The transition from compressive stress

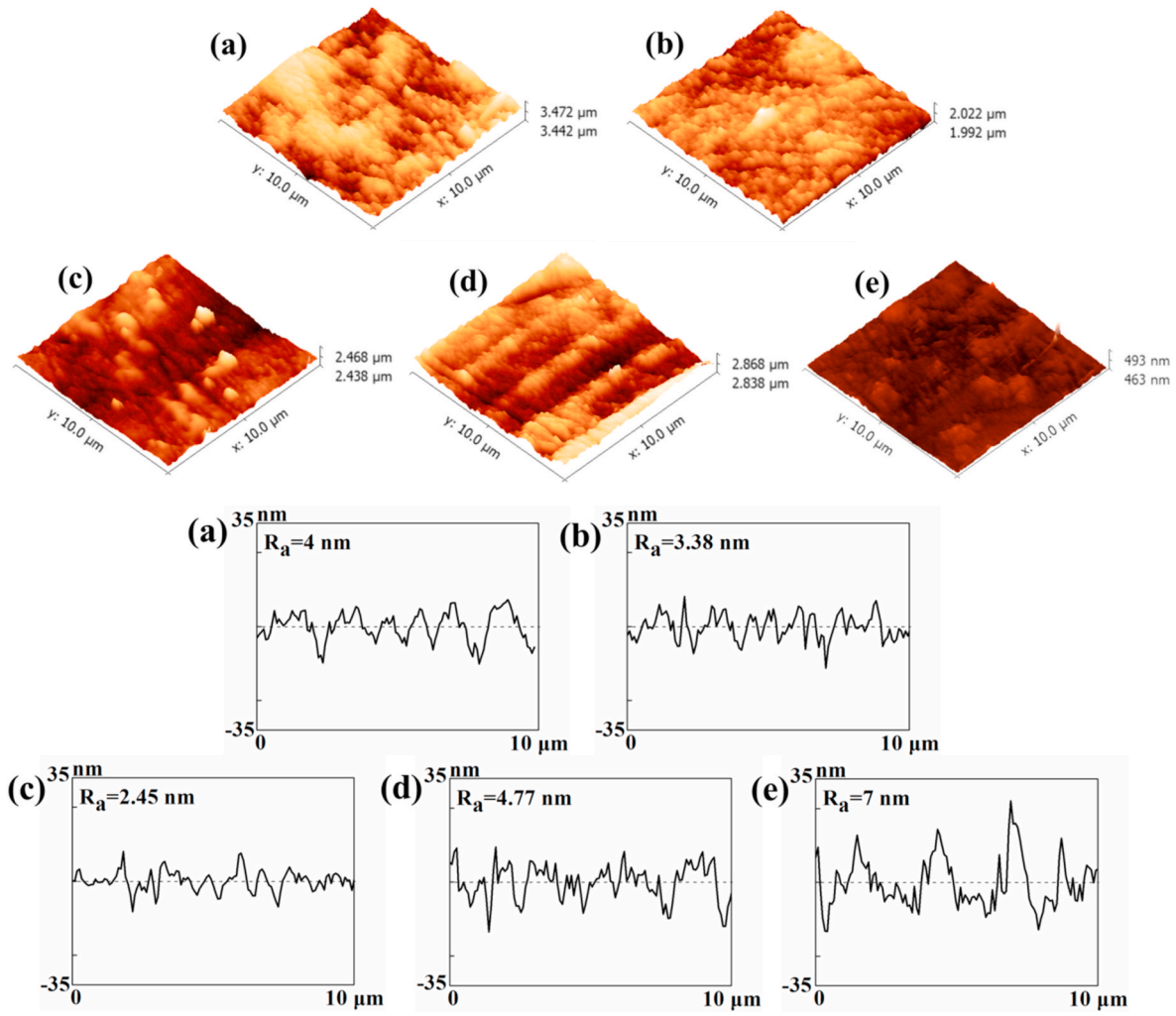

Fig. 2. AFM images and line roughness of (CrAlTiNbV)N_x coatings deposited at various substrate biases: (a) -36 V, (b) -66 V, (c) -96 V, (d) -126 V, and (e) -156 V.

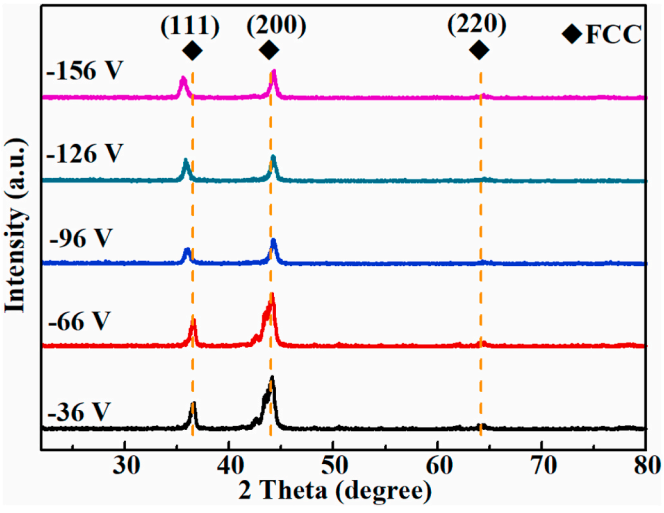

Fig. 3. XRD patterns of (CrAlTiNbV)N_x coatings versus substrate bias.

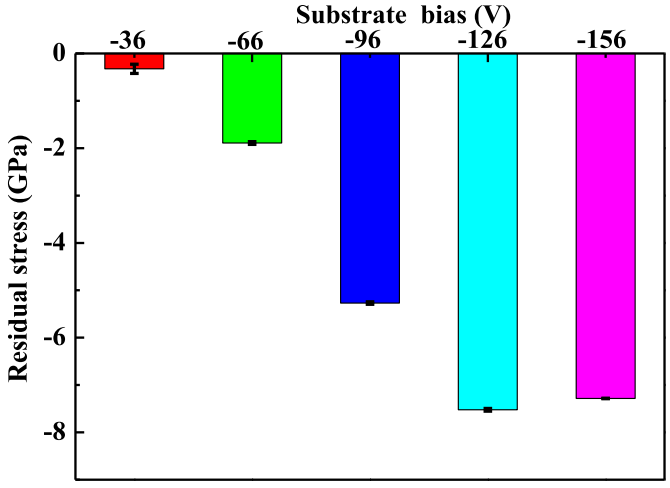

Fig. 4. Residual stress of (CrAlTiNbV)N_x coatings as a function of substrate bias.

to tensile stress is related to the gas pressure, substrate bias, coating thickness and chemical composition during the deposition process [27, 28]. In terms of transition metal nitride coatings, there exist two mechanisms for the generation of compressive stress and tensile stress, that is, the growth-induced point defects due to atomic peening, and the formation of voids owing to surface roughness and shadowing effects, respectively [27]. Besides, the compressive stress caused by the intra-column incorporation of defects and the tensile stress owing to the attractive force between the columns will grow competitively in

preparation process. As the substrate bias increases, the atom mobility and defect density in coatings are increased owing to the enhancement of ion bombardment, thus, more interstitial atoms and ions are generated, which can enlarge the compressive stress of the coating [29].

3.3. Mechanical properties

Fig. 5 displays the hardness and elastic modulus results. As the substrate bias increases, the hardness and elastic modulus of the coating gradually increase until it achieves a maximum of approximately 35.53 GPa and 354.5 GPa at -156 V, respectively. According to the above analysis, increasing the substrate bias can improve the compactness and intrinsic compressive stress of the coating. The above factors contribute to the increase of coating hardness [30]. First of all, the energy of ions bombarding the coating surface as well as the plasma density increase accompanied by the increase of substrate bias, which increases the probability of ions introducing defects and the mobility of atoms. These defects can become the second place for the formation of crystal nuclei, and atoms are easy to move to equilibrium positions, which can eliminate voids and defects in the coating. And then, it can refine the crystal grains and dense coating microstructure, thereby increasing the hardness of the coating [31]. Besides, as mentioned above, the compressive residual stress comes from the incorporation of internal defects, which will hinder the plastic flow during the deformation process, thereby increasing the hardness of the coating [29]. Although a higher hardness of the coating is obtained, it is also important to evaluate its toughness. Fig. 6 shows the trend of the ratios of H to E and H^3 to E^2 varies the substrate bias. The values of H/E and H^3/E^2 can represent for the resistance to wear and plastic deformation, respectively [32]. The H/E and H^3/E^2 values increase as the bias increases from -36 V to -156 V, which reveal an increase in resistance to wear and plastic deformation. In addition, the S-156 sample owns the most excellent properties against plastic deformation among all samples.

The adhesive behavior of coating is usually investigated by a scratch test [33]. Fig. 7 exhibits the adhesion strength of the coatings fabricated at varying substrate biases. Plots of friction coefficient and friction force in term of normal load are displayed in Fig. 7(a–e) and the average adhesion strength taken by three measurements is shown in Fig. 7 (f). The sudden change in the slope of friction coefficient is used as the criterion to determine the adhesion strength of the coating, indicating the peeling of the coating from the substrate. Based on this, the critical load of (CrAlTiNbV)N_x coatings under various substrate biases is approximately 89 N, 85 N, 76.5 N, 75 N, and 72 N, respectively, indicating the decrease of adhesion strength.

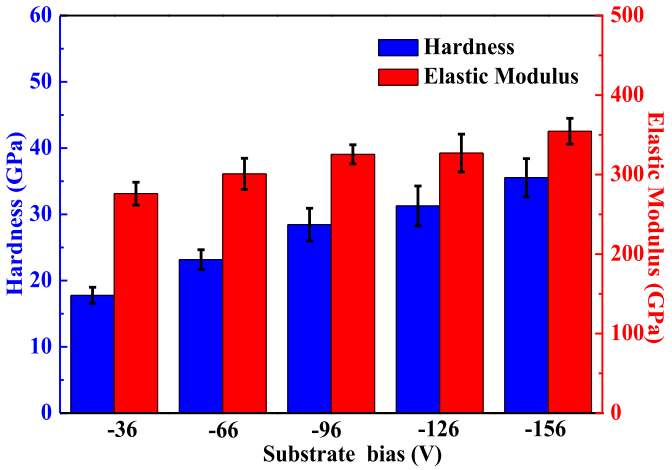

Fig. 5. Hardness and Elastic modulus of (CrAlTiNbV)N_x coatings.

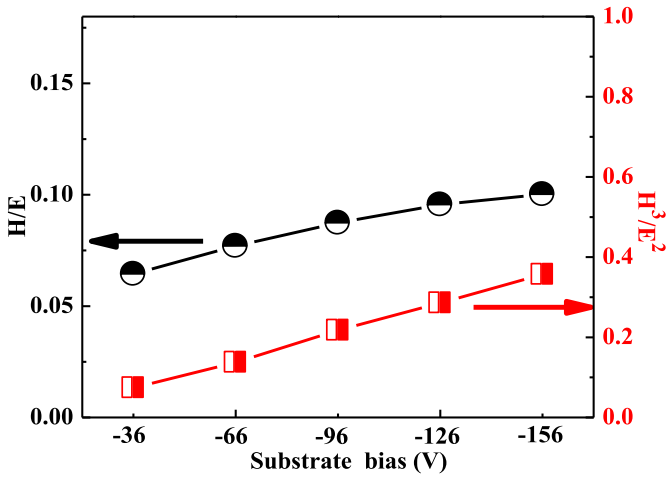

Fig. 6. H/E and H^3/E^2 values of (CrAlTiNbV)N_x coatings.

3.4. Wettability properties

The wettability and compatibility of the liquid on the solid surface have a crucial influence on the lubricating performance under the condition of solid-liquid composite lubrication [34]. Fig. 8 and Fig. 9 show the optical photographs and the contact angle values of 4050# oil to study the wettability of the oil on the steel substrate and (CrAlTiNbV)N_x coatings surface. The contact angle of 4050# oil on the steel substrate surface is the largest, but the contact angle on the surface of the coating becomes smaller. The results show that 4050# oil has good wettability and compatibility on the coating surface and wets the coating surface more easily, which is conducive to combining the advantages of solid coating and liquid lubricating oil and exerting the advantages of synergistic lubrication.

3.5. Tribological properties

Fig. 10 displays the friction coefficient of (CrAlTiNbV)N_x coatings deposited at varying biases in 4050# aviation lubricant. It can be apparently observed that the friction coefficient of coatings fluctuates between 0.06 and 0.11 in 4050# aviation oil at varying biases in the atmospheric environment. Among all the samples, the friction coefficient of the steel substrate in 4050# aviation oil is relatively stable, and the average friction coefficient is close to 0.09. At the beginning, the friction coefficients for the coating deposited at varying biases are high, in the range of 0.1–0.2, which can be ascribed to the oxide layer covering the surface of the coating and the counterpart [35]. With prolonged time, the wear track becomes wider, which reduces the nominal surface contact pressure, thereby contributing to a decrease in the friction coefficient. As the coating deposited on the substrate, the average friction coefficient of the coating is lower than that of the steel substrate in 4050# aviation oil under lower substrate biases (-36 V, -66 V, -96 V), whereas the S-96 sample exhibits the lowest average friction coefficient (about 0.06). When the substrate bias continues to increase, the friction coefficient of the coating is larger than that of the steel substrate, and the S-126 and S-156 sample reach the largest friction coefficient value (0.11). These results display that the coatings deposited at lower substrate bias possess a good anti-friction effect, whereas the S-96 sample exhibits a more effective anti-friction effect. The increase of the surface roughness and stress concentration can exacerbate the friction and thus obtain a higher friction coefficient [36]. As the substrate bias increases, the compressive residual stress of the coating gradually increases, higher residual stress values (-7.52 GPa, -7.28 GPa) are obtained at higher biases (-126 V, -156 V), which can account for a higher friction coefficient.

Fig. 11 exhibits the result of wear rate of the steel substrate and

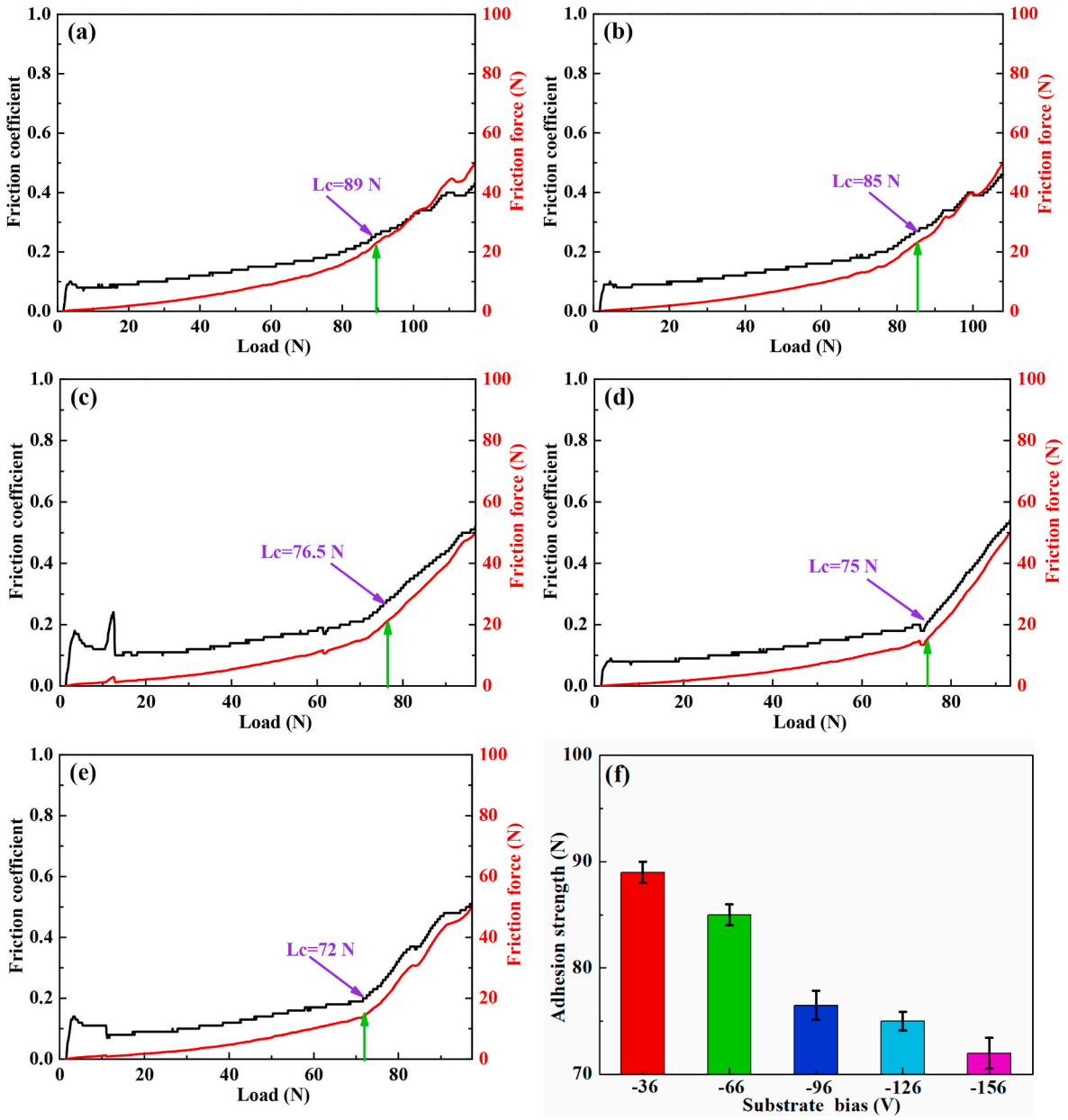

Fig. 7. (a–e) Plots of friction coefficient and friction force in term of normal load and (f) adhesion strength of $(CrAlTiNbV)N_x$ coatings deposited at various substrate biases.

$(CrAlTiNbV)N_x$ coatings deposited at varying biases in 4050# aviation lubricant. The wear resistances of $(CrAlTiNbV)N_x$ coatings under higher biases (-126 V, -156 V) are improved than that of deposited under lower biases (-36 V, -66 V, -96 V), and the S-156 sample owns the lowest wear rate (8.7×10^{-9} $mm^3/N{\cdot}m$), which is an order of magnitude lower than that of the steel substrate. The decrease in wear rate is attributed to the dense microstructure of the coatings prepared by varying substrate biases. Fig. 12 displays the 3D images of wear tracks for the steel substrate and $(CrAlTiNbV)N_x$ coatings fabricated at varying biases after 2 h wear test. It can be seen that abrasion grooves appear on the surface to varying degrees regardless of the change in bias, indicating its abrasive wear mechanism. This is mainly due to the fact that a large number of formed abrasive grains gather at the friction interface and slide on the friction surface to produce furrows, thereby intensifying the wear process. Among them, a wider and deeper wear track for the steel substrate can be observed in 4050# aviation lubricant, indicating a higher wear rate. However, the wear tracks of the coating for the S-126 and S-156 sample are relatively narrow and shallow, implying a lower wear rate. The increase in the substrate bias results in a denser microstructure and a large residual stress of the coating, which in turn increases the hardness of the coating. The wear mechanism becomes less abrasive as the H^3/E^2 value increases, which can effectively enhance the anti-wear capability of abrasion wear. Furthermore, it can be clearly seen that the deposition of $(CrAlTiNbV)N_x$ coatings on the steel substrate is an effective way to provide a decreased wear rate by controlling the suitable parameters in preparation process. The above results prove that the $(CrAlTiNbV)N_x$ coatings can be regarded as protective coatings for aviation bearing steel applications.

4. Conclusions

In summary, the influence of the substrate bias on the microstructure and mechanical properties of $(CrAlTiNbV)N_x$ coatings are investigated. The tribological properties of the coatings are explored in aviation

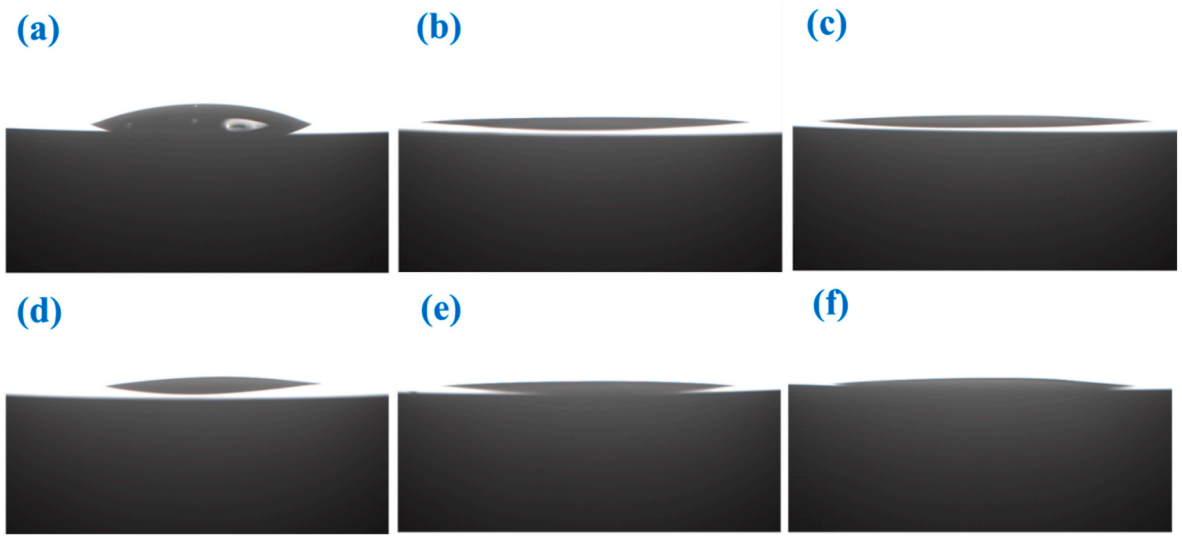

Fig. 8. The optical photographs of the oils on the steel substrate (a) and (CrAlTiNbV)N_x coatings surface fabricated at varying substrate biases: (b) -36 V, (c) -66 V, (d) -96 V, (e) -126 V, and (f) -156 V.

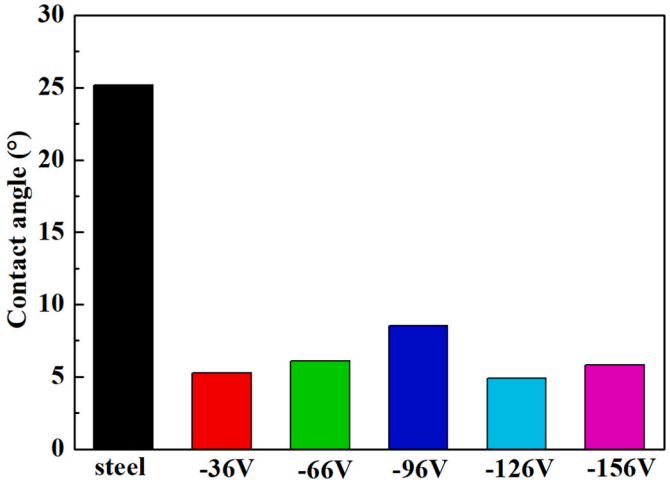

Fig. 9. The contact angle values of the oils on the steel substrate and (CrAlTiNbV)N_x coatings surface.

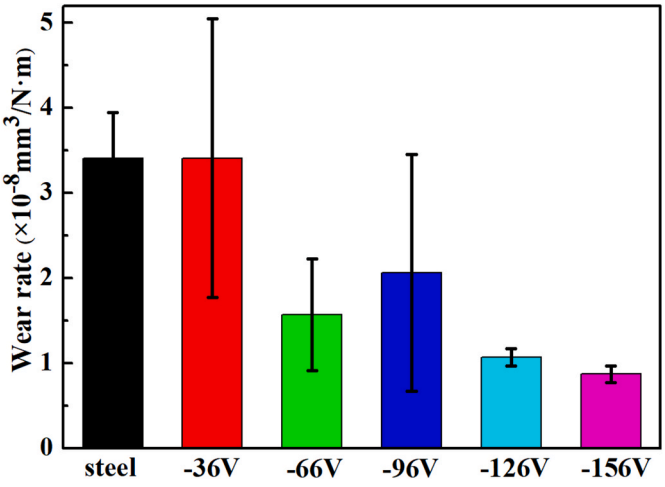

Fig. 11. Wear rate of (CrAlTiNbV)N_x coatings deposited at varying substrate biases.

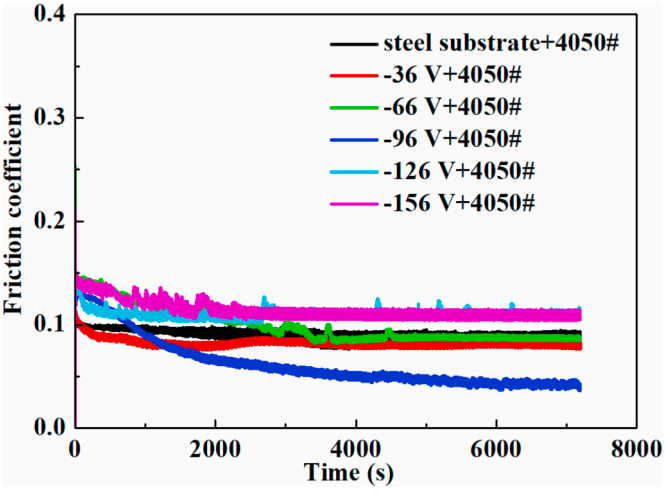

Fig. 10. Friction coefficient of (CrAlTiNbV)N_x coatings in 4050# aviation lubricant.

lubricant to make up for the lack of study on solid-liquid composite lubrication. The main conclusions obtained are drawn:

(1) FESEM and AFM results show that (CrAlTiNbV)N_x coatings present cross-section columnar structure and dome-like surface morphology. The coating transforms into a dense nanocrystalline structure with increasing substrate bias.
(2) All coatings predominantly possess a strong (200) orientation. However, when the substrate bias increases, the (111) orientation is enhanced.
(3) The compressive residual stress of the coating gradually increases with the increase of substrate bias, in the range of -0.3 to -7.5 GPa, and is greatly affected by the enhancement of ion bombardment under higher bias. On the contrary, the adhesion strength of the coating decreases with increasing substrate bias.
(4) As the increase of substrate bias, the (CrAlTiNbV)N_x coatings present increasing hardness and attain 35.53 GPa at -156 V thanks to the dense microstructure and large compressive stress of the coating. Similarly, the H/E and H^3/E^2 values increase as the bias increases from -36 V to -156 V, indicating an increase in the resistance to wear and plastic deformation.

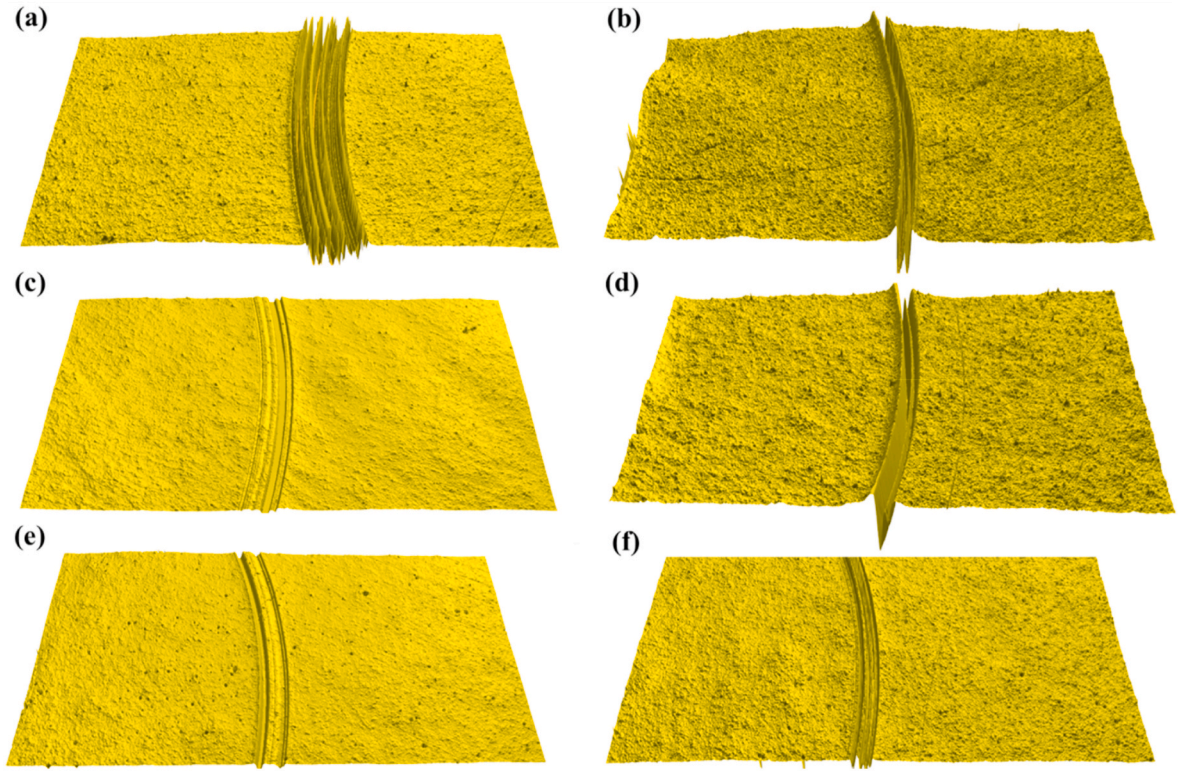

Fig. 12. Wear track morphology of (a) steel substrate and (b–f) $(CrAlTiNbV)N_x$ coatings fabricated at varying substrate biases: (b) -36 V, (c) -66 V, (d) -96 V, (e) -126 V, and (f) -156 V.

(5) Friction tests demonstrate that the friction coefficient of the coating decreases first, whereas the S-96 sample exhibits the lowest average friction coefficient (about 0.06), and then increases as a consequence of larger surface roughness and excessive stress concentration. However, a better wear resistance of the coating is presented on the samples prepared under a higher bias. Namely, the S-156 sample owns the lowest wear rate (8.7×10^{-9} $mm^3/N{\cdot}m$), which can be attributed to the contribution of dense microstructure and excellent resistance to wear and plastic deformation for the coating prepared under higher bias.

Declaration of competing interest

The authors declare that they have no known competing financial interests or personal relationships that could have appeared to influence the work reported in this paper.

Acknowledgments

The authors gratefully acknowledge the financial support of National Natural Science Foundation of China (51835012, 51805515), the National Key R&D Plan of China (No. 2018YFB0703803), the program of "Science & Technology International Cooperation Demonstrative Base of Metal Surface Engineering along the Silk Road (2017D01003)," and CAS "Light of West China".

References

[1] H. Bhadeshia, Steels for bearings, Prog. Mater. Sci. 57 (2012) 268–435, https://doi.org/10.1016/j.pmatsci.2011.06.002.

[2] Y.S. Kim, H.J. Park, S.C. Mun, E. Jumaev, S.H. Hong, G. Song, J.T. Kim, Y.K. Park, K.S. Kim, S.I. Jeong, Y.H. Kwon, K.B. Kim, Investigation of structure and mechanical properties of TiZrHfNiCuCo high entropy alloy thin films synthesized by magnetron sputtering, J. Alloys Compd. 797 (2019) 834–841, https://doi.org/10.1016/j.jallcom.2019.05.043.

[3] R. Chen, Z.B. Cai, J.B. Pu, Z.X. Lu, S.Y. Chen, S.J. Zheng, C. Zeng, Effects of nitriding on the microstructure and properties of VAlTiCrMo high-entropy alloy coatings by sputtering technique, J. Alloys Compd. 827 (2020) 153836, https://doi.org/10.1016/j.jallcom.2020.153836.

[4] A. Xia, R. Dedoncker, O. Glushko, M.J. Cordill, D. Depla, R. Franz, Influence of the nitrogen content on the structure and properties of MoNbTaVW high entropy alloy thin films, J. Alloys Compd. 850 (2021) 156740, https://doi.org/10.1016/j.jallcom.2020.156740.

[5] C.H. Lai, K.H. Cheng, S.J. Lin, J.W. Yeh, Mechanical and tribological properties of multi-element (AlCrTaTiZr)N coatings, Surf. Coating. Technol. 202 (2008) 3732–3738, https://doi.org/10.1016/j.surfcoat.2008.01.014.

[6] S. Das, S. Guha, P.P. Das, R.K. Ghadai, Analysis of morphological, microstructural, electrochemical and nano mechanical characteristics of TiCN coatings prepared under N_2 gas flow rate by chemical vapour deposition (CVD) process at higher temperature, Ceram. Int. 46 (2020) 10292–10298, https://doi.org/10.1016/j.ceramint.2020.01.023.

[7] R. Dedoncker, P. Djemia, G. Radnoczi, F. Tetard, L. Belliard, G. Abadias, N. Martin, D. Depla, Reactive sputter deposition of CoCrCuFeNi in nitrogen/argon mixtures, J. Alloys Compd. 769 (2018) 881–888, https://doi.org/10.1016/j.jallcom.2018.08.044.

[8] N.A. Khan, B. Akhavan, C.F. Zhou, H.R. Zhou, L. Chang, Y. Wang, Y.P. Liu, M. M. Bilek, Z.W. Liu, High entropy nitride (HEN) thin films of $AlCoCrCu_{0.5}FeNi$ deposited by reactive magnetron sputtering, Surf. Coating. Technol. 402 (2020) 126327, https://doi.org/10.1016/j.surfcoat.2020.126327.

[9] H.W. Chang, P.K. Huang, J.W. Yeh, A. Davison, C.H. Tsau, C.C. Yang, Influence of substrate bias, deposition temperature and post-deposition annealing on the structure and properties of multi-principal-component (AlCrMoSiTi)N coatings, Surf. Coating. Technol. 202 (2008) 3360–3366, https://doi.org/10.1016/j.surfcoat.2007.12.014.

[10] Y.C. Lin, S.Y. Hsu, R.W. Song, W.L. Lo, Y.T. Lai, S.Y. Tsai, J.G. Duh, Improving the hardness of high entropy nitride $(Cr_{0.35}Al_{0.25}Nb_{0.12}Si_{0.08}V_{0.20})N$ coatings via tuning substrate temperature and bias for anti-wear applications, Surf. Coating. Technol. 403 (2020) 126417, https://doi.org/10.1016/j.surfcoat.2020.126417.

[11] A.D. Pogrebnjak, I.V. Yakushchenko, O.V. Bondar, V.M. Beresnev, K. Oyoshi, O. M. Ivasishin, H. Amekura, Y. Takeda, M. Opielak, C. Kozak, Irradiation resistance, microstructure and mechanical properties of nanostructured (TiZrHfVNbTa)N coatings, J. Alloys Compd. 679 (2016) 155–163, https://doi.org/10.1016/j.jallcom.2016.04.064.

[12] Y. Xu, G. Li, Y. Xia, Synthesis and characterization of super-hard AlCrTiVZr high-entropy alloy nitride films deposited by HiPIMS, Appl. Surf. Sci. 523 (2020) 146529, https://doi.org/10.1016/j.apsusc.2020.146529.

[13] X.L. Lu, C.X. Zhang, C. Wang, X.J. Cao, R. Ma, X.D. Sui, J.Y. Hao, W.M. Liu, Investigation of $(CrAlTiNbV)N_x$ high-entropy nitride coatings via tailoring nitrogen flow rate for anti-wear applications in aviation lubricant, Appl. Surf. Sci. 557 (2021) 149813, https://doi.org/10.1016/j.apsusc.2021.149813.

[14] J.J. Wang, S.Y. Chang, F.Y. Ouyang, Effect of substrate bias on the microstructure and properties of (AlCrSiNbZr)N_x high entropy nitride thin film, Surf. Coating. Technol. 393 (2020) 125796, https://doi.org/10.1016/j.surfcoat.2020.125796.
[15] W.L. Lo, S.Y. Hsu, Y.C. Lin, S.Y. Tsai, Y.T. Lai, J.G. Duh, Improvement of high entropy alloy nitride coatings (AlCrNbSiTiMo)N on mechanical and high temperature tribological properties by tuning substrate bias, Surf. Coating. Technol. 401 (2020) 126247, https://doi.org/10.1016/j.surfcoat.2020.126247.
[16] L. Patnaik, S.R. Maity, S. Kumar, Mechanical and tribological assessment of composite AlCrN or a-C: Ag-based thin films for implant application, Ceram. Int. 47 (2021) 6736–6752, https://doi.org/10.1016/j.ceramint.2020.11.016.
[17] N. Behravan, A. Farhadizadeh, S. Ghasemi, A. Khademi, H. Shojaei, H. Ghomi, The pressure dependence of structure and composition of sputtered AlCrSiTiMoO high entropy thin film, J. Alloys Compd. 852 (2021) 156421, https://doi.org/10.1016/j.jallcom.2020.156421.
[18] J.A. Floro, E. Chason, R.C. Cammarata, D.J. Srolovitz, Physical origins of intrinsic stresses in Volmer-Weber thin films, MRS Bull. 27 (2002) 19–25, https://doi.org/10.1557/mrs2002.15.
[19] P.P. Cui, W. Li, P. Liu, K. Zhang, F.C. Ma, X.H. Chen, R. Feng, P.K. Liaw, Effects of nitrogen content on microstructures and mechanical properties of (AlCrTiZrHf)N high-entropy alloy nitride films, J. Alloys Compd. 834 (2020) 155063, https://doi.org/10.1016/j.jallcom.2020.155063.
[20] D.C. Tsai, Y.L. Huang, S.R. Lin, S.C. Liang, F.S. Shieu, Effect of nitrogen flow ratios on the structure and mechanical properties of (TiVCrZrY)N coatings prepared by reactive magnetron sputtering, Appl. Surf. Sci. 257 (2010) 1361–1367, https://doi.org/10.1016/j.apsusc.2010.08.078.
[21] S.C. Liang, Z.C. Chang, D.C. Tsai, Y.C. Lin, H.S. Sung, M.J. Deng, F.S. Shieu, Effects of substrate temperature on the structure and mechanical properties of (TiVCrZrHf)N coatings, Appl. Surf. Sci. 257 (2011) 7709–7713, https://doi.org/10.1016/j.apsusc.2011.04.014.
[22] W.J. Shen, M.H. Tsai, Y.S. Chang, J.W. Yeh, Effects of substrate bias on the structure and mechanical properties of ($Al_{1.5}CrNb_{0.5}Si_{0.5}Ti$)$N_x$ coatings, Thin Solid Films 520 (2012) 6183–6188, https://doi.org/10.1016/j.tsf.2012.06.002.
[23] J. Pelleg, L.Z. Zevin, S. Lungo, N. Croitoru, Reactive-sputter-deposited TiN films on glass substrates, Thin Solid Films 197 (1991) 117–128, https://doi.org/10.1016/0040-6090(91)90225-M.
[24] P. Patsalas, C. Gravalidis, S. Logothetidis, Surface kinetics and subplantation phenomena affecting the texture, morphology, stress, and growth evolution of titanium nitride films, J. Appl. Phys. 96 (2004) 6234–6246, https://doi.org/10.1063/1.1811389.
[25] P.K. Huang, J.W. Yeh, Effects of substrate bias on structure and mechanical properties of (AlCrNbSiTiV)N coatings, J. Phys. D Appl. Phys. 42 (2009) 115401, https://doi.org/10.1088/0022-3727/42/11/115401.
[26] A.D. Pogrebnjak, I.V. Yakushchenko, A.A. Bagdasaryan, O.V. Bondar, R. Krause-Rehberg, G. Abadias, P. Chartier, K. Oyoshi, Y. Takeda, V.M. Beresnev, O.V. Sobol, Microstructure, physical and chemical properties of nanostructured (Ti-Hf-Zr-V-Nb)N coatings under different deposition conditions, Mater. Chem. Phys. 147 (2014) 1079–1091, https://doi.org/10.1016/j.matchemphys.2014.06.062.
[27] G. Abadias, P. Guerin, In situ stress evolution during magnetron sputtering of transition metal nitride thin films, Appl. Phys. Lett. 93 (2008) 111908, https://doi.org/10.1063/1.2985814.
[28] G. Abadias, W.P. Leroy, S. Mahieu, D. Depla, Influence of particle and energy flux on stress and texture development in magnetron sputtered TiN films, J. Phys. D Appl. Phys. 46 (2013), 055301, https://doi.org/10.1088/0022-3727/46/5/055301.
[29] M.H. Hsieh, M.H. Tsai, W.J. Shen, J.W. Yeh, Structure and properties of two Al-Cr-Nb-Si-Ti high-entropy nitride coatings, Surf. Coating. Technol. 221 (2013) 118–123, https://doi.org/10.1016/j.surfcoat.2013.01.036.
[30] H.T. Hsueh, W.J. Shen, M.H. Tsai, J.W. Yeh, Effect of nitrogen content and substrate bias on mechanical and corrosion properties of high-entropy films $(AlCrSiTiZr)_{100-x}N_x$, Surf. Coating. Technol. 206 (2012) 4106–4112, https://doi.org/10.1016/j.surfcoat.2012.03.096.
[31] D.C. Tsai, S.C. Liang, Z.C. Chang, T.N. Lin, M.H. Shiao, F.S. Shieu, Effects of substrate bias on structure and mechanical properties of (TiVCrZrHf)N coatings, Surf. Coating. Technol. 207 (2012) 293–299, https://doi.org/10.1016/j.surfcoat.2012.07.004.
[32] H.R. Ma, Q. Miao, G.H. Zhang, W.P. Liang, Y. Wang, Z.W. Sun, H. Lin, The influence of multilayer structure on mechanical behavior of TiN/TiAlSiN multilayer coating, Ceram. Int. 47 (2021) 12583–12591, https://doi.org/10.1016/j.ceramint.2021.01.117.
[33] X.D. Sui, G.J. Li, C.J. Jiang, K. Wang, Y.J. Zhang, J.Y. Hao, Q. Wang, Improved toughness of layered architecture TiAlN/CrN coatings for titanium high speed cutting, Ceram. Int. 44 (2018) 5629–5635, https://doi.org/10.1016/j.ceramint.2017.12.210.
[34] Z. Yan, D. Jiang, Y.L. Fu, D. Qiao, X.M. Gao, D.P. Feng, J.Y. Sun, L.J. Weng, H. Z. Wang, Vacuum tribological performance of WS_2-MoS_2 composite film against oil-impregnated porous polyimide: influence of oil viscosity, Tribol. Lett. 67 (2019) 1–10, https://doi.org/10.1007/s11249-018-1101-3.
[35] M.M. Yan, X.Y. Wang, H.B. Zhou, J. Liu, S.T. Zhang, Y. Lu, J.Y. Hao, Microstructure, mechanical and tribological properties of graphite-like carbon coatings doped with tantalum, Appl. Surf. Sci. 542 (2021) 148404, https://doi.org/10.1016/j.apsusc.2020.148404.
[36] J.Q. Wang, H.J. Zhao, W. Huang, X.L. Wang, Investigation of porous polyimide lubricant retainers to improve the performance of rolling bearings under conditions of starved lubrication, Wear 380–381 (2017) 52–58, https://doi.org/10.1016/j.wear.2017.03.008.